Diamond & Related Materials 133 (2023) 109692

Contents lists available at ScienceDirect

Diamond & Related Materials

journal homepage: www.elsevier.com/locate/diamond

A 3D diamond dosimeter with graphitic surface connections

A. Porter [a,*], K. Kanxheri [b], I. Lopez Paz [a], A. Oh [a], L. Servoli [b], C. Talamonti [c,d]

[a] University of Manchester, United Kingdom
[b] INFN, Perugia, Italy
[c] University of Florence, Italy
[d] INFN, Firenze, Italy

ARTICLE INFO

Keywords:
Diamond dosimetry graphitic 3D detector CVD

ABSTRACT

A new prototype 3D diamond dosimeter featuring laser-written graphitic surface connections and bonding pads has been tested. Diamond substrates are of interest to medical dosimetry as they are closer to bodily tissue equivalence than other solid-state materials. The device in this work was made with a polycrystalline chemical vapour deposition diamond substrate (pCVD) was laser processed to have internal 3D electrode columns and surface connections including the wire-bonding pads to make an all-carbon detector, with no metal-diamond interfaces. Polycrystalline diamond can be produced with a larger area and cheaper cost than single crystal diamond, but has a relatively slow timing response due to charge trapping defects inside the substrate. To mitigate material defects, 3D sensor technology has been proposed. The 3D design has charge collection electrodes as columns spaced inside the material bulk perpendicular to the surface. When compared to the conventional 'planar' sensor design, the 3D arrangement decouples the charge collection distance from the thickness of the substrate, theoretically allowing for more efficient charge collection and the active volumes have smaller dimensions. The laser writing process used for the 3D columns was extended to make graphitic surface connections replacing conventionally used metal bonding contacts between the 3D graphitic columns and readout electronics. The removal of metal-diamond contacts in the detector volume reduces the distortion of the electric field close to the surface of the diamond. The prototype was tested using a laboratory X-ray tube and a clinical Elekta Synergy BM LINAC and was found to have dose-rate independence consistent with previous 3D diamond dosimeters but with lower operating voltages, the lowest being +6 V. Lower operating voltage is attributed to the removal of the electric field distortion at diamond-metal interfaces. This paper proposes the first implementation of an all-carbon 3D diamond dosimeter using a polycrystalline substrate.

1. Introduction

Diamond is the hardest natural material known to man. It has been used to make ionising radiation detectors, particularly in high-radiation environments such as particle physics experiments, nuclear reactors and radiotherapy. Diamond has inherent radiation hardness, low leakage current, high breakdown voltage, fast charge mobilities and thermal stability. This has warranted the interest and development of diamond as a sensor technology [1,2]. Of particular interest in medical dosimetry is tissue equivalence, as the effective mass of carbon is close to that of bodily tissue ($Z_{carbon} = 6 \approx Z_{tissue} = 7.14$) [3]. As novel and emerging treatments are being developed, such as FLASH radiotherapy (dose rates of 40–60 Gy [4]), devices representative of human tissue with a stable fast time response in a high dose rate environment are more desirable.

The charge collection electrodes of a detector are conventionally placed on the surface of the diamond substrate. For example, on the front and back sides (planar) or two perpendicular sides (Schottky diode). Alternatively, the present state-of-the-art configuration has electrodes structures can be placed inside the diamond substrate, named a '3D' detector [5–7]. For conventional planar detectors, the separation of the electrodes is directly coupled to and limited by the thickness of the substrate, as they are typically fabricated on the top and back plane of the diamond. A 3D device has columnar electrodes inscribed within the bulk of the sensitive material, decoupling the inter-electrode distance from the substrate thickness as shown in Fig. 1.

3D diamond devices are made using synthetic diamond substrates, produced by chemical vapour deposition (CVD). Synthetic production allows for larger wafer size, with a uniform crystal structure, at cheaper

* Corresponding author.
E-mail address: alice.porter@manchester.ac.uk (A. Porter).

https://doi.org/10.1016/j.diamond.2023.109692
Received 9 November 2022; Received in revised form 28 December 2022; Accepted 8 January 2023
Available online 18 January 2023

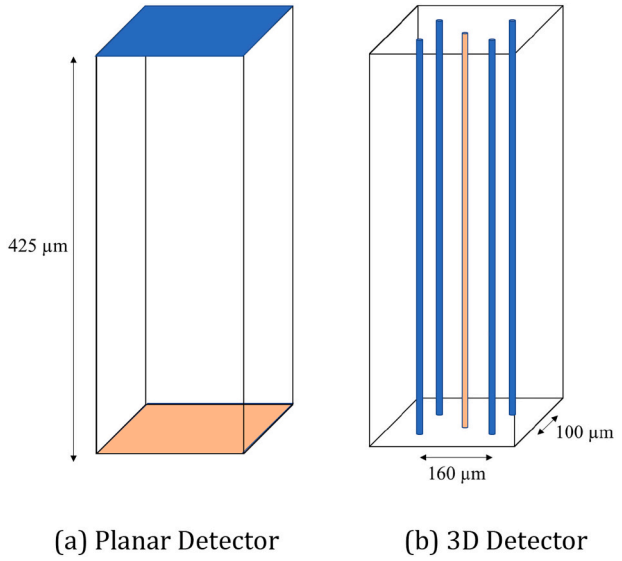

Fig. 1. Illustration of the arrangement of the bias (blue) and collection (orange) electrodes in planar (a) and an elementary 3D cell (b) configurations. The planar layout has surface electrodes whose distance is governed by the thickness of the diamond. The 3D columnar electrodes are through the depth of the diamond, so the separation can be much smaller than a planar structure of the same thickness.

material cost than naturally sourced diamonds. There are two distinct grades of CVD diamond: single crystal (scCVD) and polycrystalline (pCVD). Dosimeters made with scCVD diamond films exposed to photon beams are characterised by a stable, fast and reproducible response [8,9]. However, an important disadvantage of scCVD diamonds for practical applications in radiotherapy dosimetry is the maximum achievable wafer size (1 cm diameter), paired with higher material cost, which makes the construction of large area dosimeters unfeasible. Due to their lower cost, pCVD diamonds have been proposed as suitable candidates for radiotherapy dosimetry. The current state-of-art technology demonstrates that high quality pCVD wafers with up to 2.5 cm^2 surface area can be produced with promising dosimetric properties [10–13]. There are concerns about response instability and slow rise and fall times of pCVD diamond detectors [14,15]. This is due to a significant amount of native deep and shallow defects within the crystal structure, which can trap charge carriers, at room temperature, affecting the device response stability. While the improvement of pCVD diamond substrate stability can be obtained by pre-irradiation to occupy charge traps prior to dosimetric measurements [3], 3D fabrication has been demonstrated as an alternative method for improving the detector response time. The significant reduction of the inter-electrode distance in a 3D design reduces the probability of a charge carrier becoming trapped before reaching the collection electrode [16]. The small dimensions of the sensor offered by the 3D design are known to limit the effects of the high density of diamond relative to bodily tissue [17,18]. By means of this innovative fabrication process it is possible to exploit the advantages and minimise the deficiencies of the pCVD substrate [19].

The fabrication of a 3D diamond device utilises the conversion of diamond to ohmically conducting graphite under the action of a laser beam. As the diamond crystal is transparent to the laser beam wavelength, the beam spot can be focused inside the diamond's bulk. The diamond to graphite transition occurs from multiphoton absorption from a sufficiently photon dense beam spot. The beam spot is translated from the back plane towards the top surface of the diamond to create a continuous graphitic column. The characteristics of the graphitic material depend on the wavelength, intensity and pulse duration (typically on the femto- to nanosecond scale) of the laser beam. The standard connection between the graphitic electrodes and the external readout circuitry is via metallic surface contacts, typically with physical deposition of chromium-gold [20]. In this work, surface graphitisation was used in place of metallisation, directly reducing the presence of extra metallic components in the detector package. Reducing metallic components in the detector will also help to minimise X-ray scatter, therefore is of interest in precision photon radiotherapy, where highly conformal X-ray doses are desirable. While previous studies have explored planar diamond dosimeters with non-metal diamond-like-carbon electrical contacts made by graphite sputtering [17], or with graphitic wires leading to metal contacts [16], none have considered direct wire-bonding to graphitic surface connections made by laser inscription. The performance of diamond detectors used as dosimeters strongly depends on the diamond-metal interfaces [17,21]. Therefore, in addition to providing stable electronic contacts on the diamond surface, an approach has been proposed to remove the diamond-metal interface. The following discussion is on the implementation of a 3D diamond design with surface graphitisation and contacts on a pCVD substrate.

2. Methods

2.1. Experimental apparatus

2.1.1. Device under test

The device under test (DUT) is a 3D all-carbon sensor fabricated within a 5 × 5 × 0.5 mm^3 pCVD detector grade diamond sample produced in the framework of the 3DOSE INFN experiment. Every pixel in the detector matrix has a sensitive region of 500 × 560 × 425 μm^3 consisting of elementary cells of 100 × 160 × 425 μm^3, as illustrated in Fig. 1b. An elementary cell is defined by the volume between graphitic electrode columns, with 4 bias columns in the corners and one collection electrode in the centre. The laser processing was performed with different pulse length lasers for the internal and surface features to account for diffraction losses as described in reference [22]. The graphitic electrodes were inscribed by action of a femto-second Ti:Sapphire laser of 70 fs pulse length, 1 kHz repetition rate and a 1 µJ pulse energy.

The electrodes and external circuitry were connected using surface graphitisation in place of conventional physical deposition metallisation. Graphitic paths were chosen in order to produce better electrical connection to the inscribed columns than a metal alternative. The surface graphitisation process used a Nd:YAG laser beam with 8 ns pulse length focused on the surface plane at a repetition rate of 5 kHz and operated between 45 and 55 % of the maximum power of 40 µJ [22]. The process produced lines in the diamond surface with 6 µm in width and depth [23]. These thin graphitic conductive paths cause less distortion to the electric field within the diamond bulk, which is the active region of the detector. The pixels were connected to larger square regions of blanket surface graphitisation, as can be seen in Fig. 2. These areas provide surfaces for wire bond connections with allowance for multiple bonding attempts, as a graphite-metal wire-bonding is a non-standard procedure with a low success rate.

The diamond was mounted on a PCB with SMA connections to the readout apparatus. The mounted PCB was encapsulated in a 14 × 14 × 14 cm^3 block of PMMA, as shown in Fig. 4. The depth at which the PCB is housed can be altered on this model of PMMA phantom and is discussed further below. Connected to the readout on the detector package was a 4-channel fast interface bipolar *CAEN Els Tetramm* picoammeter with integrated voltage bias source, which provided both bias voltage to the sample and current monitoring of the readout channel. A *LabView* custom interface was created to monitor the current signal. The *Tetramm* sampled the current every 1 µs and the recorded current was averaged over every 0.5 s window.

2.1.2. Laboratory set-up

The assembled device was set up inside a *Votsch VT-4010* environmental chamber to minimise external influences during initial characterisation. The nozzle of an *Amp-Tek Mini-X* X-ray source was directed at

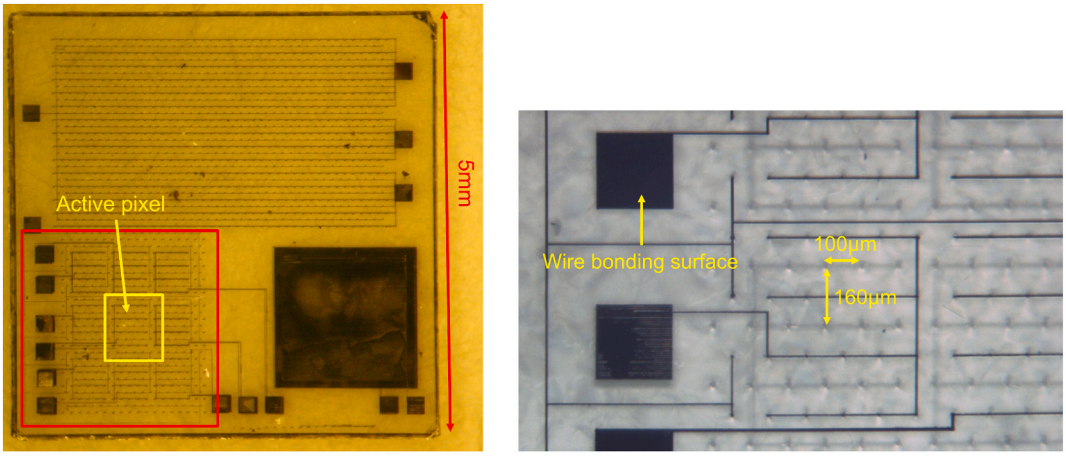

Fig. 2. Optical microscope images of the (a) whole graphitised diamond and (b) a close up of the region with 3D pixels. The region of interest (red) is split into an array of 9 3D pixels. The wire-bonding pads can be seen as the smaller filled squares around the surface. The horizontal lines are the surface connections between the 3D electrodes. The pixel that was successfully bonded to the external circuitry is highlighted in yellow.

the pixel of interest in the device through the wall of the chamber. The PCB was mounted with 1 cm of PMMA above in the phantom, as shown in Fig. 4a. This was to minimise the air gap around the detector's sensitive area, but suitably close to receive direct irradiation from the nozzle. Standard co-axial cabling connected the DUT to the readout apparatus outside the environmental chamber. The source-target distance was not altered throughout the testing period. The source was used to induce a current to be measured in the DUT. The X-ray source was set to a nominal 30 kV operation voltage, with the beam current varied between 60 and 180 µA.

2.1.3. Clinical testing set-up

To test the detector in a clinical environment, the detector was set up on the patient bed of an *Elekta Synergy BM* LINAC treatment beam set to 6 MV, as shown in Fig. 3, at Radiotherapy Unit of the University Hospital in Florence, Italy. The detector was assembled inside a PMMA phantom, at 10 cm depth as is the standardised depth of solid water for medical X-ray beam calibration [24] as shown in Fig. 4b. The phantom was placed upon a motorised movable stage (single step precision 210 nm) resting on the patient bed. The detector was aligned 100 cm from the source using the LINAC system's light guide lines. Lengths of ethernet cabling, around 10 m, were used to communicate to the *Tetramm* from outside the treatment room, kept behind a concrete door. Otherwise, the current in the detector was monitored using the same data-acquisition system as detailed for the laboratory. The dose-rate supplied by this LINAC is calibrated to have a conversion of 1 MU/min to 1 cGy/min.

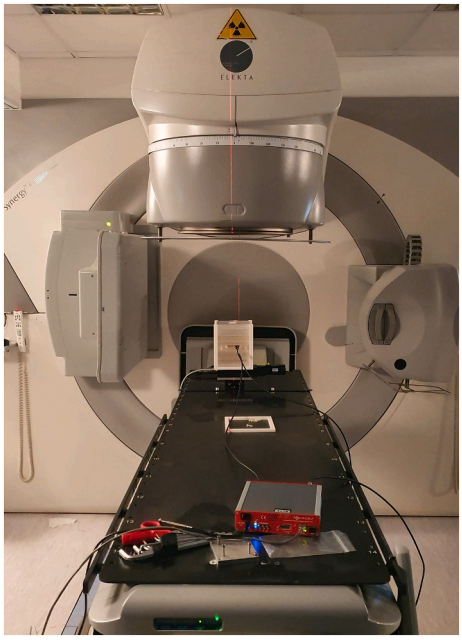

Fig. 3. The *Elekta Synergy BM* LINAC used to test the DUT. The PMMA phantom containing the diamond device can be seen on the patient bed below the source aperture of the LINAC beam.

2.2. Experimental tests

2.2.1. Voltage scan

To characterise the device's optimum working voltage point, the DUT's applied bias voltage was varied whilst exposed to a fixed X-ray energy and rate in the laboratory. The induced current within the DUT from the incident X-rays was recorded for measured for equal exposure times of 30 s at each bias voltage point. The voltage polarity was tested in the available positive domain up to +70 V. Beyond this value the detector displayed exponentially increasing currents associated with electrical breakdown. In the interest of preserving the device's function, voltages above +70 V were not used. This test was repeated for varying tube currents for the same peak voltage available from the X-ray tube.

2.2.2. Dose rate linearity

For an ideal dosimeter, the detector's response should be independent of the dose rate. It is therefore important to quantify the device's response linearity to a range of dose-rates and to parametrise the extent the device deviates from linearity. The detector was tested at a range of dose rates in the laboratory and at the University Hospital. In the laboratory, the current setting of the X-ray beam tube was used as a proxy for dose rate. As the dose rate from the X-ray tube is known to be stable up to 150 µA, only measurements up to that value have been considered. This protocol was then repeated for the clinical dose-rates available at Florence University for two bias voltage values, +10 V and +60 V, in the range found to be operational in the laboratory.

To verify the detector's linear response to dose rate, the current measurement data was fitted with a linear function specified by Fowler and Laub [25,26] given as.

$$I = I_{dark} + K \cdot D^{\Delta}, \quad (1)$$

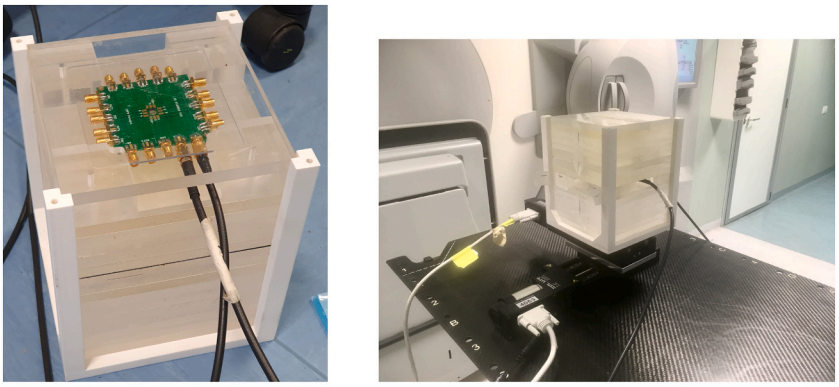

(a) (b)

Fig. 4. The PMMA phantom used to mount the detector. In the laboratory the PCB was placed in the top layer as shown in (a). For clinical testing there is 10 cm of PMMA or solid water on top of the mounting slot and the phantom is on a movable stage as shown in (b).

where the current measured in the detector is I, the leakage (or dark) current is I_{dark}, the dose rate is D, the detector sensitivity is parameterised by K and Δ is the correlation factor of the data shown, which indicates the linearity of the response.

2.2.3. Beam profile

By moving the detector in steps in one axial direction on the motorised stage, the change in induced current can be attributed to a position relative to the beam profile. As the beam profile is resolved along one dimension, the highest measured photo-current value along the axis is assumed to be the centre of the beam. Using this method, the beam profile was measured on the perpendicular axis for two different nominal beam sizes available on the LINAC (8×8 mm^2 and 16×16 mm^2) and two different movement step sizes (0.2 mm and 0.5 mm).

3. Results and discussion

The results show that this device with only graphitic surface connections, the first of its kind, is functional and exhibits key characteristics suitable for use as a radiation dosimeter. As discussed below, there is value to the detector performance by the replacement of conventional metallisation to surface graphitisation for a 3D diamond dosimeter. Metal components cause interface phenomena, so reducing metallic content in the detector package is of interest within the scope of medical physics as it will reduce perturbations to dose measurements [21]. The implementation is a proof of concept for an all-carbon 3D diamond device, with scope for further design refinements.

3.1. Voltage scan

A standard 500 μm planar diamond device reaches full charge collection efficiency at around 500 V (about 1 V/μm) with operation ranges 100–1000 V; by comparison, 3D diamond devices, built with the same substrate thickness, require 40–50 V of bias to fully collect the generated charge [19,27]. This is important for a prospective dosimeter as full charge collection is necessary for a proper assessment of radiation dose. As shown in Fig. 5, the detector was operational at voltages as low as ≈6 *V*. This indicates that the 3D region was active during testing with bias voltages lower than previous devices with metal contacts. This is likely to be attributed to the removal of metal surface structures reducing the interference with the electric field distribution inside the active region. The diamond-metal interface plays an important role in the operation voltage. The difference between diamond and metal work functions favours the flow of electrons from lower to higher work function regions. As a consequence an effective junction is created, as one material becomes slightly positive charged while the other slightly

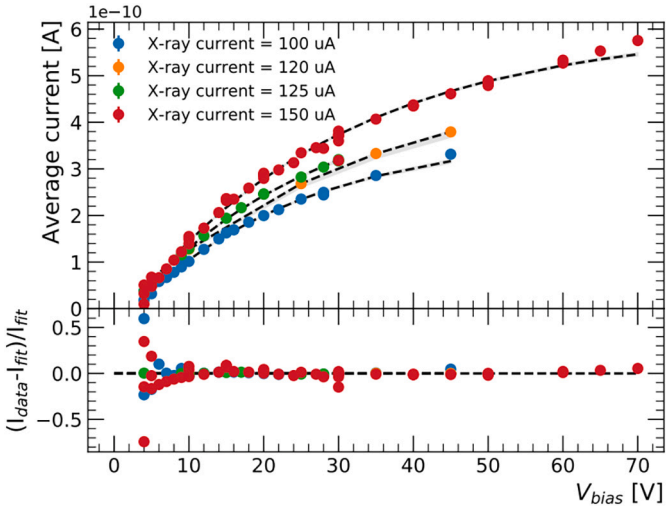

Fig. 5. The measured current in the detector for different applied bias voltages. The colours correspond to the beam current supplied to the X-ray tube. The deviation from the fit is shown in the bottom plot.

negative. When the detector is exposed with ionising radiation, charges accumulate within the crystal. These immobile carriers generate their own electric field which opposes an applied field produced by an external polarisation voltage, in this case the bias voltage. This reduces the resulting electric field strength within the detector's sensitive volume, and subsequently the efficiency of charge collection. Graphitic paths in place of metal have been proposed to solve the issue of polarisation at the diamond surface, and the observed lower operational voltage supports this reasoning. Low voltage operation may be an attractive consideration in the interest of patient and practitioner safety.

3.2. Dose-rate linearity

The current response to a range X-ray tube beam currents is shown in Fig. 6 and the measurements taken in the clinical setting are shown in Fig. 7. Both sets of data were fitted with the function shown in Eq. (1). The fitting parameters for both datasets are shown in Table 1. The device shows dose-rate linearity comparable to studies of similar 3D diamond structures [12]. The linearity factor Δ is stable across the bias voltages and in both the laboratory and clinical setting. The lowest bias voltage tested was +6 V with this value showing consistent linearity factor and a reasonable signal-to-noise ratio (as indicated by the comparable

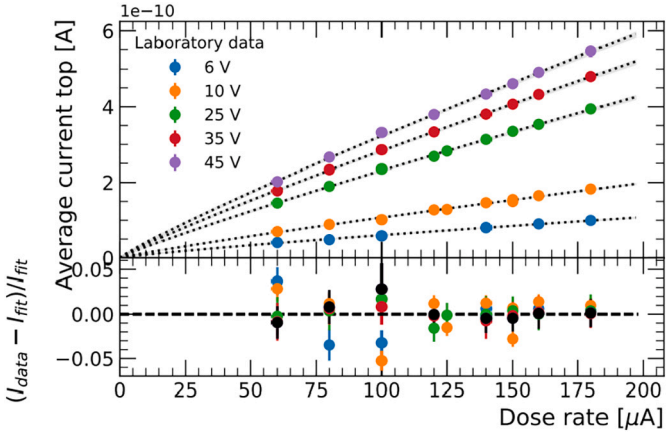

Fig. 6. The measured current in the device for different applied bias voltages as a function of X-ray tube beam current. The data is fitted with a linear function for each voltage. The deviations from linearity are shown in the lower portion of the plot with the average deviation between the voltages with black markers.

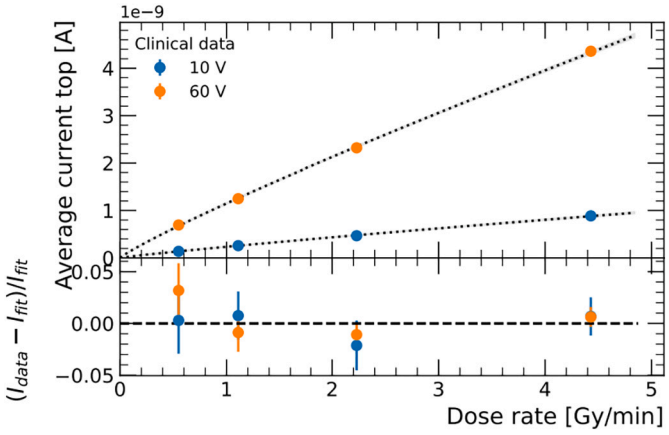

Fig. 7. The measured current in the device for low and high applied bias voltages as a function dose-rate. The data is fitted with a linear function for each voltage. The deviations from linearity are shown in the lower portion of the plot.

Table 1
The linearity factors and sensitivities of the 3D pixel extracted from the measured response in (a) the laboratory setting and (b) the clinical setting.

(a)

V_b [V]	Δ	K [nC/μA]
+6	0.999	0.842 ± 0.015
+10	0.999	0.893 ± 0.011
+25	0.999	0.900 ± 0.020
+35	0.999	0.895 ± 0.019
+45	0.999	0.894 ± 0.018

(b)

V_b [V]	Δ	K [nC/Gy]
+10	0.999	53.3 ± 0.9
+60	0.999	53.5 ± 0.6

sensitivity). This is an improvement as previously the lowest bias voltage this linearity factor was recorded with 3D diamond dosimeters was +10 V. This suggests that there has been no compromise on the quality of dosimetric measurement by the removal of the metal-diamond bonding pad. In fact, lower voltage operation is available with usable sensitivity.

The device showed suitable current responses in terms of linearity with respect to dose-rate both in the clinical and laboratory settings, thus confirming the suitability of such a device for dosimetric measurements, especially at low voltages. With the application of the innovative interdigitated electrodes, diamond detectors with very small sensitive areas but with relatively large sensitive volumes were fabricated, leading to highly segmented devices with a high signal-to-noise ratio. However, the definition of the exact sensitive volume is unclear as there is no definite boundary to the 3D pixel structure. To understand what is the expected sensitivity from the diamond active volume contribution, some calculations are necessary to indicate if the entire generated charge is being considered correctly, or underestimated or overestimated. The dimensions of the single pixel used for measurements, as reported in Paragraph 1.1, define a sensitive volume as 0.14 mm^3. The density of diamond is known to be 3510 kg/m^3, hence the mass of a pixel is 49.1 × 10^{-8} kg. 1 Gy of absorbed dose corresponds to an energy absorption of 1 J/kg. Therefore, 1 Gy of dose delivered to 49.1 × 10^{-8} kg of diamond mass absorbs 49.1 × 10^{-8} J of energy, corresponding to 3.06 × 10^{12} eV. The energy needed to produce an electron-hole pair in diamond is 13 eV/ion pair [3]. Therefore, 3.06 × 10^{12} eV of energy produces 2.36 × 10^{11} electron-hole pairs. If considering an ideal situation within which the entirety of the generated charges take part in photoconduction, 1 Gy of absorbed dose generates 37.8 nC of charge, or the maximal single pixel sensitivity is 37.8 nC/Gy. From the sensitivity values shown in Table 1, there is a larger amount of current collected than anticipated for the volume of the connected pixel. This suggests that there could be charge carriers collected from outside the single pixel volume. To clarify this point, the next iteration of test structures should be better isolated from the surrounding diamond substrate. This could be obtained by inclusion of a guard ring structure and through all 9 pixels in the matrix being properly connected, to localise the extent of the electric field around the central pixel considered in this work. The new structure may improve the definition of detector sensitivity as there will be no contributions to the signal from outside the isolated region [28]. Nevertheless, despite the possible uncertainty on sensitive volume and the removal of traditional metal readout architecture, the consistency of the device's linear response at both laboratory and clinical dose rates are encouraging.

3.3. Beam profiles

The beam profile was measured for two different beam sizes (8 × 8 mm^2 and 16 × 16 mm^2) and two different motor step sizes (0.2 mm and 0.5 mm) and the resulting profiles are shown in Fig. 8. Comparing results from procedures with differing travelling step sizes will show if the detector response is affected by volume averaging [29,30]. The average difference between the profiles measured of the 8 × 8 mm^2 beam is (0.20 ± 0.61 %) and of the 16 × 16 mm^2 beam is (0.09 ± 0.62)%. This shows there is no significant difference between measuring the beam with different step sizes. This is indicative of volume averaging, which is expected as the step size is less than the dimensions of the active pixel. The beam profiles of the DUT were compared to the same profiles measured by a commercial PTW microDiamond dosimeter. The 200 μm step size was then plotted with data on the same LINAC with a commercial PTW diamond dosimeter for reference and is shown for both beam sizes in Fig. 9. The comparison of the measured beam profiles shows that relative to the PTW, the DUT overestimates the beam width. The active pixel in the DUT has a surface area of 0.28 mm^2 and volume 0.14 mm^3. Relative to the PTW dosimeter (4 mm^2 active measurement area, 0.004 mm^3 active volume) it is expected for the DUT to be overestimating the penumbra as it has a larger sensitive volume. Therefore, it is recommended that volume be reduced in future iterations, perhaps with fewer 3D cells per pixel, so that a single pixel can have an active volume comparable to the PTW and a smaller area.

Further development and testing of 3D diamond dosimeters with

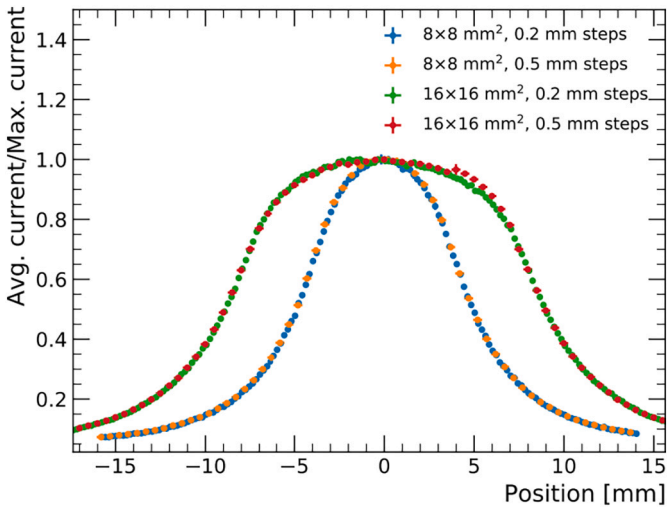

Fig. 8. The measured LINAC beam profiles shown as current as a function of position about the centre. The profiles show different beam sizes each with 2 different step sizes.

surface graphitisation should be done to fully evaluate the potential for higher resolution clinical beam measurements. This would involve the inclusion of a guard-ring structure around the matrix of sensitive pixels, that has shown to reduce charge sharing from regions outside that defined and isolated by a guard-ring structure [31]. Reducing the pixel volume and clearly defining its boundary with a guard ring could be a convincing solution to improve the spatial resolution in a 3D diamond device, making it comparable to the commercial diamond dosimeters in this respect.

4. Conclusion

A prototype of dosimeter based on 3D diamond technology has been built and tested. The device is all-carbon, up to the aluminium wire bonding to connect to readout. The device operates at lower voltages (+6 V) than previous 3D diamond devices with similar internal structures. This is attributed to the removal of the metal-diamond interface on the surface of the device. The device shows dose-rate linearity and time resolution consistent with other commercial clinical diamond dosimeters. The spatial resolution and detector sensitivity are overestimated in these measurements as the single pixel volume was not adequately isolated. Despite this the performance was comparable to previous 3D diamond dosimeters with metallic surface connections. It is therefore a worthwhile venture to further pursue the development of such devices.

CRediT authorship contribution statement

A. Porter: Formal analysis, Investigation, Data curation, Writing – original draft. **K. Kanxheri:** Investigation, Resources, Software, Writing – review & editing. **I. Lopez Paz:** Visualization, Data curation. **A. Oh:**

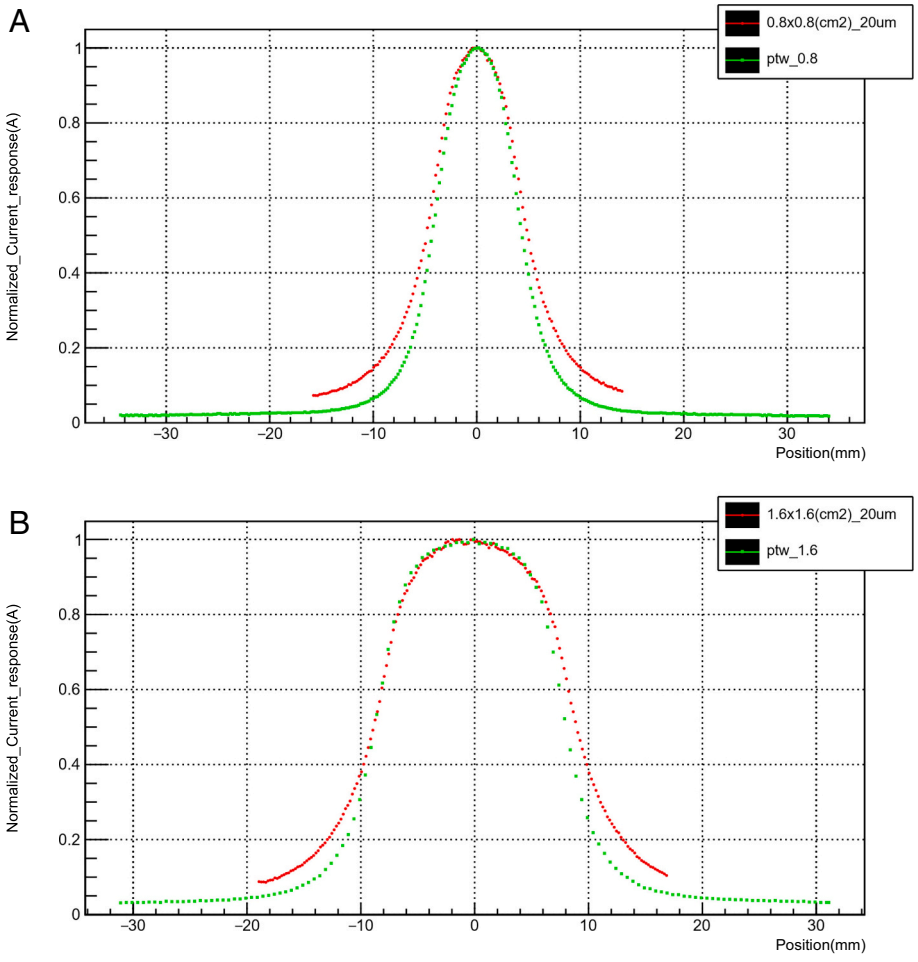

Fig. 9. Beam profile for (a) 0.8 × 0.8 cm^2 and (b) 1.6 × 1.6 cm^2 beam sizes and with a 0.2 mm stage step size. The measurement made with a PTW dosimeter is shown in green and the DUT is in red.

Project administration, Supervision, Conceptualization. **L. Servoli:** Resources, Conceptualization, Project administration, Writing – review & editing. **C. Talamonti:** Resources, Supervision, Data curation, Writing – review & editing.

Declaration of competing interest

Alice Porter reports a relationship with Science and Technology Facilities Council that includes: travel reimbursement.

Data availability

Data will be made available on request.

Acknowledgements

This work has been carried out within the 3Dose project INFN-CSN5. AP would like to thank STFC CDN+ for their support by travel bursary. The authors would also like to acknowledge the positive environment given by the RD42 Collaboration.

References

[1] M. Franklin, A. Fry, K. Gan, S. Han, H. Kagan, S. Kanda, D. Kania, R. Kass, S. Kim, R. Malchow, F. Morrow, S. Olsen, W. Palmer, L. Pan, F. Sannes, S. Schnetzer, R. Stone, Y. Sugimoto, G. Thomson, C. White, S. Zhao, Nucl. Instrum. Methods Phys. Res., Sect. A 315 (1992) 39–42.
[2] C. White, W. Dulinski, D. Fujino, K.K. Gan, R. Gilman, S. Han, J. Hassard, A. Howard, H. Kagan, S. Kanda, D. Kania, R. Kass, S.K. Kim, G. Kumbartski, M. H. Lee, K. Lister, R. Malchow, S. Margetides, L.S. Pan, P. Rutt, F. Sannes, S. Schnetzer, S.V. Somalwar, J. Straver, R. Stone, R. Tesarek, G.B. Thomson, W. Trischuk, Y. Sugimoto, G.B. Thomson, P. Weilhammer, C. White, S. Zhao, Nucl. Inst. Methods Phys. Res. A 351 (1994) 217–221. ISSN 01689002.
[3] M. Bucciolini, C. De Angelis, C. Talamonti, in: Diamond Detectors for Dosimetry vol 8, 2014, pp. 229–248. ISBN 9780444536334.
[4] J.D. Wilson, E.M. Hammond, G.S. Higgins, K. Petersson, Front. Oncol. (2020) 9. ISSN 2234-943X.
[5] S.I. Parker, C.J. Kenney, J. Segal, Nucl. Instrum. Methods Phys. Res., Sect. A 395 (1997) 328–343. ISSN 01689002.
[6] F. Bachmair, L. Bäni, P. Bergonzo, B. Caylar, G. Forcolin, I. Haughton, D. Hits, H. Kagan, R. Kass, L. Li, A. Oh, S. Phan, M. Pomorski, D.S. Smith, V. Tyzhnevyi, R. Wallny, D. Whitehead, A 3D diamond detector for particle tracking, Nucl. Instrum. Methods Phys. Res., Sect. A 786 (2015) 97–104.
[7] K. Kanxheri, L. Servoli, A.M. Oh, F. Munoz Sanchez, G. Forcolin, S. Murphy, A. Aitkenhead, C. Moore, A. Morozzi, D. Passeri, S. Lagomarsino, S. Sciortino, J. Instrum. 12 (2017).
[8] S. Almaviva, I. Ciancaglioni, R. Consorti, F. Notaristefani, C. Manfredotti, M. Marinelli, E. Milani, A. Petrucci, G. Prestopino, C. Verona, G. Verona Rinati, Diam. Relat. Mater. 19 (2010) 217–220.
[9] C. Moignier, D. Tromson, F. Marsolat, M. Agelou, M. Pomorski, R. Woo, J. M. Bourbotte, F. Moignau, D. Lazaro, A. Mazal, L. De Marzi, J. Hernández, Phys. Med. Biol. 62 (2017) 5417–5439.
[10] C. Talamonti, High- quality polycrystalline CVD diamond for conformal radiotherapy applications, in: Proceedings of 10th International Conference on Large Scale Applications and Radiation Hardness of Semiconductor Detectors — PoS(RD11), 2012, p. 015. ISSN 18248039.
[11] A. Bartoli, I. Cupparo, A. Baldi, M. Scaringella, A. Pasquini, S. Pallotta, C. Talamonti, M. Bruzzi, J. Instrum. 12 (2017). C03052-C03052.
[12] K. Kanxheri, L. Alunni Solestizi, M. Biasini, M. Caprai, A. Dipilato, M. Iacco, M. Ionica, S. Lagomarsino, M. Menichelli, A. Morozzi, D. Passeri, S. Sciortino, C. Talamonti, C. Zucchetti, L. Servoli, J. Instrum. 13 (2018). P06006-P06006.
[13] A. Whitehead, R. Airey, C. Buttar, J. Conway, G. Hill, S. Ramkumar, G. Scarsbrook, R. Sussmann, S. Walker, Nucl. Instrum. Methods Phys. Res., Sect. A 460 (2001) 20–26. ISSN 01689002.
[14] C. De Angelis, M. Casati, M. Bruzzi, S. Onori, M. Bucciolini, Nucl. Instrum. Methods Phys. Res., Sect. A 583 (2007) 195–203.
[15] S. Lagomarsino, M. Bellini, C. Corsi, V. Cindro, K. Kanxheri, A. Morozzi, D. Passeri, L. Servoli, C.J. Schmidt, S. Sciortino, Appl. Phys. Lett. 106 (19) (2015), 193509. ISSN 0003–6951.
[16] K. Kanxheri, D. Aisa, L. Alunni Solestizi, M. Bellini, M. Caprai, C. Corsi, A. Dipilato, M. Iacco, M. Ionica, S. Lagomarsino, A. Morozzi, F. Moscatelli, D. Passeri, S. Sciortino, C. Talamonti, C. Zucchetti, L. Servoli, Nucl. Instrum. Methods Phys. Res., Sect. A 958 (2019), 162730.
[17] F. Marsolat, D. Tromson, N. Tranchant, M. Pomorski, C. Bassinet, C. Huet, S. Derreumaux, M. Chea, K. Cristina, G. Boisserie, I. Buchheit, V. Marchesi, S. Josset, A. Lisbona, D. Lazaro, R. Hugon, P. Bergonzo, J. Appl. Phys. 118 (2015), 234507.
[18] K. Kanxheri, C. Talamonti, S. Sciortino, S. Lagomarsino, M. Ionica, M. Caprai, F. Moscatelli, L. Servoli, Phys. Med. 102 (2022) 73–78. ISSN 2234-943X.
[19] C. Talamonti, K. Kanxheri, S. Pallotta, L. Servoli, Front. Phys. (2021) 9. ISSN 2296424X.
[20] F. Marsolat, D. Tromson, N. Tranchant, M. Pomorski, M. Le Roy, M. Donois, F. Moignau, A. Ostrowsky, L. De Carlan, C. Bassinet, C. Huet, S. Derreumaux, M. Chea, K. Cristina, G. Boisserie, P. Bergonzo, Phys. Med. Biol. 58 (2013) 7647–7660. ISSN 00319155.
[21] B. Górka, B. Nilsson, R. Svensson, A. Brahme, Phys. Med. Biol. 51 (2006) 3607–3623.
[22] S. Lagomarsino, M. Bellini, M. Brianzi, R. Carzino, V. Cindro, C. Corsi, A. Morozzi, D. Passeri, S. Sciortino, L. Servoli, Nucl. Instrum. Methods Phys. Res., Sect. A 796 (2015) 42–46. ISSN 01689002.
[23] S. Lagomarsino, M. Bellini, C. Corsi, S. Fanetti, F. Gorelli, I. Liontos, G. Parrini, M. Santoro, S. Sciortino, Diam. Relat. Mater. 43 (2014) 23–28. ISSN 09259635.
[24] Absorbed Dose Determination in External Beam Radiotherapy (Technical Reports Series no 398) (Vienna: INTERNATIONAL ATOMIC ENERGY AGENCY) ISBN 92-0-102200-X.
[25] J. Fowler, Radiat. Dosim. 2 (1966) 290–324.
[26] W.U. Laub, T.W. Kaulich, F. Nüsslin, Med. Phys. 24 (1997) 535–536. ISSN 00942405.
[27] S. Lagomarsino, M. Bellini, C. Corsi, F. Gorelli, G. Parrini, M. Santoro, S. Sciortino, Appl. Phys. Lett. 103 (2013), 233507-233507.
[28] M. Booth, G. Forcolin, V. Grilj, B. Hamilton, I. Haughton, S. Murphy, A. Oh, P. Salter, M. McGowan, I. Sudïc, N. Skukan, Diam. Relat. Mater. 77 (2017) 137–145. ISSN 0925-9635.
[29] W.U. Lauba, T. Wong, Med. Phys. 30 (2003) 341–347. ISSN 00942405.
[30] A. Ralston, M. Tyler, P. Liu, N. Suchowerska, D. McKenzie, Phys. Med. Biol. 59 (2014) 5873–5881. ISSN 13616560.
[31] I.A. Zahradnik, P. Barberet, D. Tromson, L. De Marzi, M.T. Pomorski, Rev. Sci. Instrum. 91 (2020), 054102. ISSN 0034–6748.